Experimental and numerical evaluations of adhesion strength and stress in TiN films deposited on ti-implanted aluminum

Ming Xu[a)]
School of Materials Science and Engineering, Shanghai Jiao Tong University, 1954 Hua Shan Road, Shanghai 200030, China

Youming Liu
School of Materials Science and Engineering, Shanghai Jiao Tong University, Shanghai 200030, China and Department of Physics and Materials Science, City University of Hong Kong, Kowloon, Hong Kong

Liuhe Li
School of Materials Science and Engineering, Shanghai Jiao Tong University, Shanghai 200030, China and 702 Department, School of Mechanical Engineering and Automation, Beijing University of Aeronautics and Astronautics, Beijing 100083, China

Xun Cai[b)] and Qiulong Chen
School of Materials Science and Engineering, Shanghai Jiao Tong University, Shanghai 200030, China

Paul K. Chu
Department of Physics and Materials Science, City University of Hong Kong, Kowloon, Hong Kong

(Received 26 July 2005; accepted 12 December 2005; published 8 February 2006)

Titanium ions were implanted into aluminum substrates at 40 kV prior to magnetron sputtering deposition of the Ti interlayer and TiN film using our custom-designed multifunctional ion implanter without breaking vacuum. An 82-nm-thick modified layer was formed between the TiN film and the substrate. The characteristics of the implanted samples were compared to those of TiN/Al and TiN/Ti/Al samples that were not preimplanted. Based on our scratch tests, the critical loading L_c of the TiN/Ti/Ti-implanted Al sample was significantly improved compared to the unimplanted TiN/Al and TiN/Ti/Al samples. Finite element analysis was conducted to simulate the scratch process to help reveal the stress distributions in the vicinity of the interlayer. The results show that the stress around the interface is largely reduced in the TiN/Ti/Ti-implanted Al sample. Consequently, the mechanical properties such as resistance to loadings are enhanced. © *2006 American Vacuum Society.* [DOI: 10.1116/1.2165657]

I. INTRODUCTION

TiN films are widely used in tools because of their high hardness, excellent wear resistance, low friction coefficient, and good chemical stability.[1–3] They are also commonly employed to improve the surface and tribological properties of materials with low hardness and poor wear resistance such as aluminum and its alloys in load-bearing applications.[4,5] Because of the large differences in the mechanical properties such as hardness and Young's modulus between Al and TiN, there is a large residual interfacial stress in TiN films deposited onto Al, resulting in low film adhesion strength and reduced scratch resistance. Plastic deformation is one of the main factors causing fracture, and the large interfacial stress is the main cause of film delamination. Among the suggested approaches to tackle the problem is the deposition of a Ti interlayer on the aluminum substrate prior to TiN film deposition, which is one of the common methods. The effects of the substrate on the mechanical properties of the deposited film have been investigated.[6,7] There have also been reports[8,9] on the effects of the interlayer on the mechanical properties of thin film, but pretreatment using ion implantation has been relatively rare.[10–12]

In this work, Ti ion implantation is first performed to produce a graded layer in the near-surface region of the Al substrate before the Ti interlayer and TiN film is deposited. Compared to the unimplanted substrate, there is a better transition from the substrate surface to the Ti interlayer with respect to the hardness and Young's modulus. This provides more structural continuity, thereby giving rise to better mechanical properties as well as resistance against larger loading and plastic deformation. In addition, stress concentration near the interfacial zone can be reduced and the adhesion strength can be improved. In our scratch tests, microscopic inspection, acoustic emission, and frictional coefficients are used simultaneously to more accurately determine the critical load L_c of the various samples. Finite element modeling (FEM) is conducted to numerically investigate the stress distributions in the film, namely, the base tensile stress σ_{xx}, shear stress τ_{xy}, and equivalent stress σ_e at the interface.

II. EXPERIMENTAL DETAILS

Pure aluminum (99.99%) specimens $15\times15\times5$ mm^3 in size were used in our experiments. The specimens were me-

a)Electronic mail: xml@sjtu.edu.cn
b)Author to whom correspondence should be addressed; electronic mail: xcai@sjtu.edu.cn

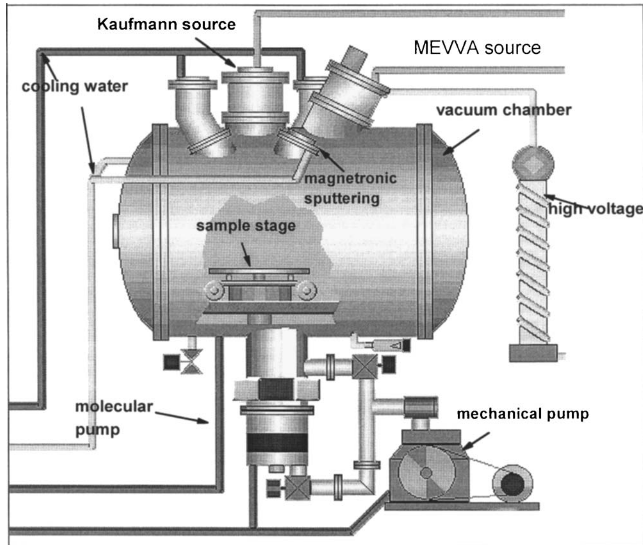

FIG. 1. Schematic of custom-designed multifunctional ion implanter.

chanically polished and ultrasonically cleaned in isopropyl alcohol for about 10 min prior to ion implantation. Ion implantation was conducted in a custom multifunctional ion implanter schematically depicted in Fig. 1.[13–15] The instrument is equipped with a dc and rf magnetron sputtering source as well as a cathodic arc metal ion source. No external heating was applied to the specimens. The sample was implanted with 40 kV titanium ions to a dose of 2×10^{17} ions/cm^2. The ion-beam current density was about 25 μA/cm^2.

After ion implantation, the sample was rotated towards the magnetron sputtering source without breaking vacuum. The background pressure in the deposition chamber was less than 2×10^{-3} Pa. The distance between the sample and magnetron sputtering source was about 4–5 cm. The target was made of 99.4% titanium, and the target voltage, current, and bias voltage were 420 V, 1.0 A, and −60 V, respectively. The nitrogen and argon gases were 99.99% pure, and the total pressure and N_2 partial pressure were 3.0×10^{-1} and 5.0×10^{-2} Pa, respectively. The detailed steps have been illustrated in Fig. 2. The thickness of the layers was determined by profilometry, and the elemental depth profiles were obtained by Auger electron spectroscopy (AES) using a sputtering rate of 4 nm/min. The structures were determined by glancing-angle x-ray diffraction (GAXRD) using a Siemens

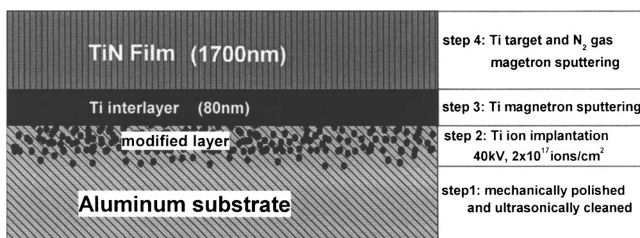

FIG. 2. Experiment steps starting from Al substrate to the Ti implantation and then deposition of Ti and TiN films.

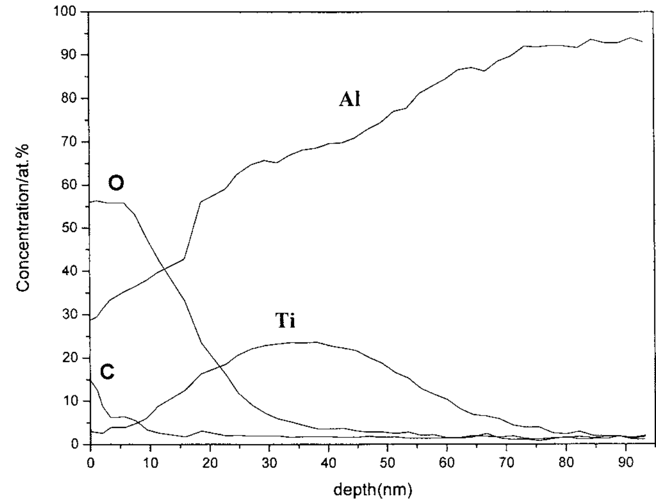

FIG. 3. Depth profiles of Al, Ti, O, and C in Ti-implanted aluminum.

Model D500 with Co $K\alpha(1+2)$ radiation at an incident angle of 1°. Nanoindentation tests were used to measure the mechanical properties of the Ti-implanted Al and TiN films of three systems. A three-sided pyramidal diamond (Berkovich) indenter (CSM Instruments) with options for continuous stiffness measurement was used. Each value was obtained by averaging five indentations to obtain good statistics. The critical load for coating failure was determined using a microscratch tester (CSEM Instruments) equipped with automatic sample translation and a Rockwell diamond indenter (50 μm radius) at a speed of 0.2%/s and a loading rate of 5000 mN/s.

III. EXPERIMENTAL RESULTS

Figure 3 shows the AES depth profiles of O, Al, C, and Ti in the Ti-implanted Al sample. The Ti profile exhibits a typical "implantlike" Gaussian distribution, implying that pure Ti ion implantation has been achieved, and Ti ions have penetrated up to a depth of 82 nm. Due to its chemical affinity, a

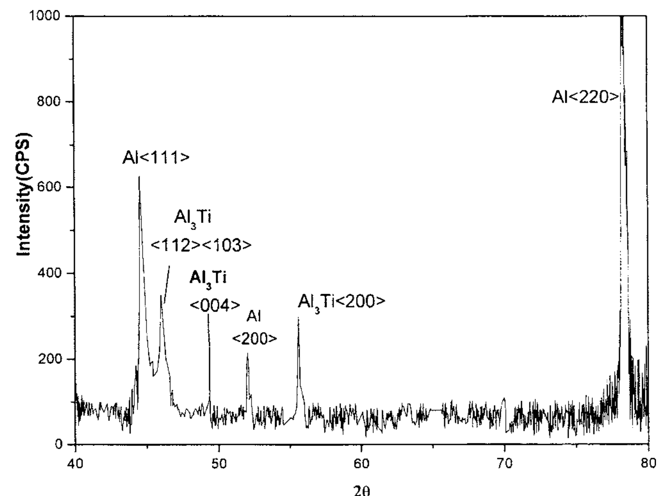

FIG. 4. GAXRD spectrum of Ti-implanted aluminum.

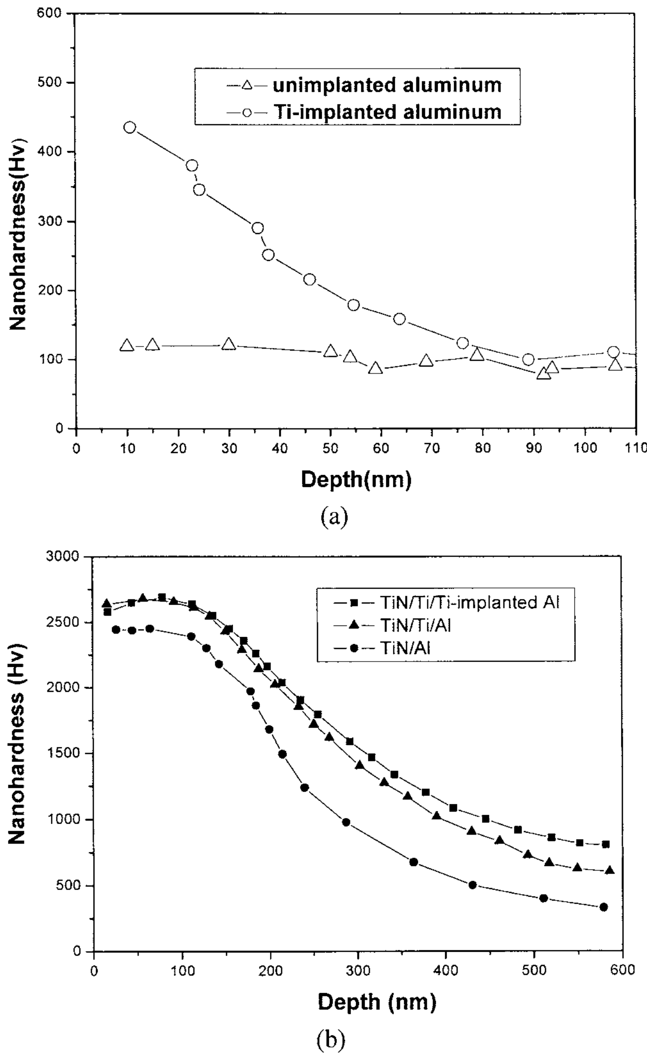

FIG. 5. (a) Nanohardness of Ti-implanted aluminum and unimplanted aluminum as a function of indentation depth; (b) nanohardness of TiN films of three systems as a function of indentation depth.

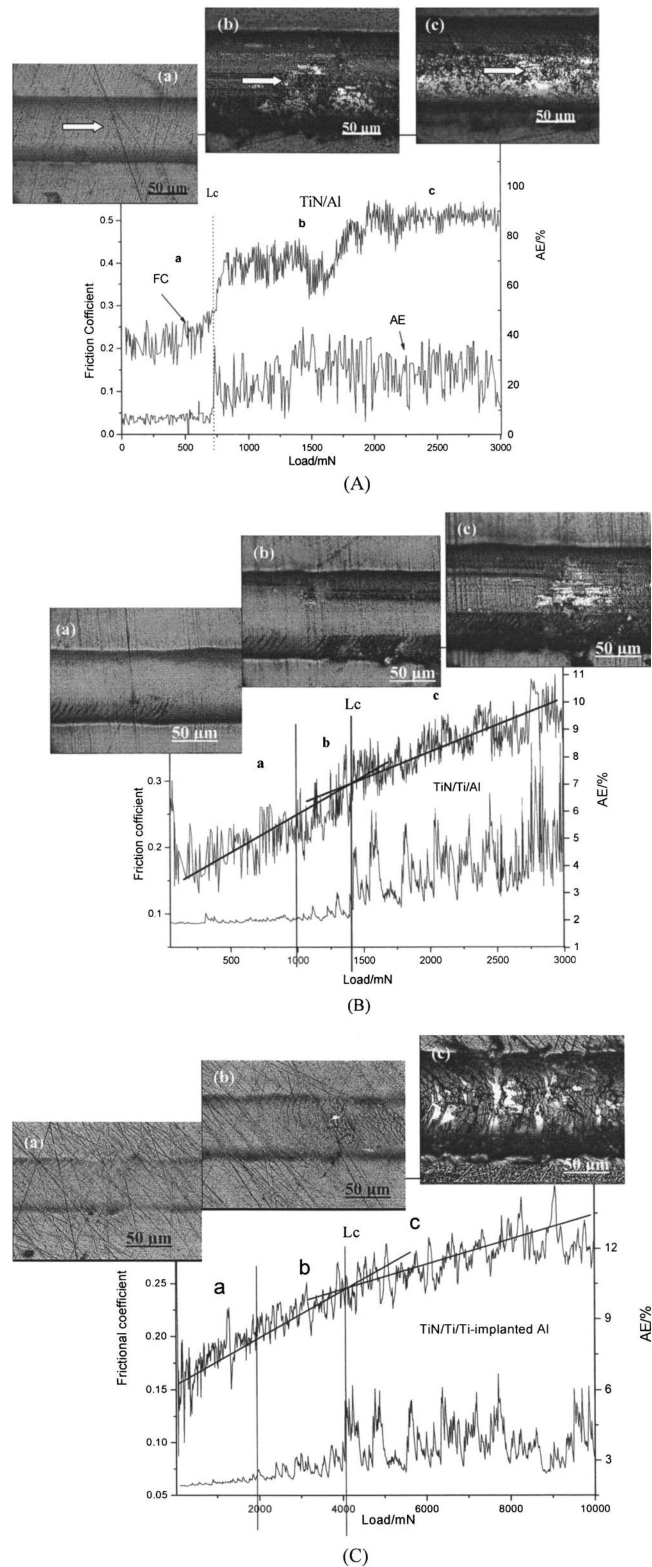

FIG. 6. Optical micrographs, friction coefficients, and acoustic emission of (A) TiN/Al-, (B) TiN/Ti/Al-, and (C) TiN/Ti/Ti-implanted Al. [(a), (b), and (c)] correspond to the regions a, b, and c of the frictional coefficient and acoustic emission graph, respectively.

certain amount of carbon is also found on the substrate surface. The presence of O results from the natural oxidation.

As shown in Fig. 4, the formation of Al_3Ti is confirmed by three obvious diffraction peaks in the GAXRD spectra. The results are consistent with other reports on titanium aluminide formation in Ti-implanted aluminum.[16,17] As the substrate material, Al is still the main phase after Ti ion implantation.

The nanohardness values of the Ti-implanted aluminum and unimplanted aluminum as a function of the contact depth (nanometer) from 10 to 110 nm are plotted in Fig. 5(a) and reveal an increase in the hardness after ion implantation. Figure 5(b) compares the nanohardness of the TiN film of TiN/Al-, TiN/Ti/Al-, and TiN/Ti/Ti-implanted Al systems. It can be observed that the decline rate of the hardness of the TiN/Ti/Ti-implanted Al sample is slower than that of TiN/Ti/Al, though the hardness of the two are almost the same in the top 200 nm. After titanium ion implantation, the tougher substrate provides the whole system with the improved ability to support loading.

In our study, we combine microscopic inspection, frictional coefficient, and acoustic emission in our microscratch tests to more accurately evaluate the adhesion strength. Fig-

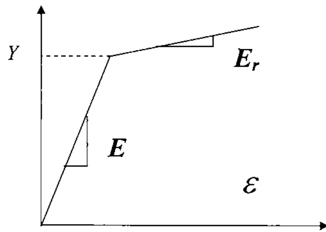

FIG. 7. Stress-strain curves of the film and the substrate in the FEM models, which is assumed as von Mises solids with discrete yielding followed by linear, isotropic work hardening.

ure 6 shows the critical loads and micrographs corresponding to the regions a, b, and c of the frictional coefficient and acoustic emission graph, respectively. The L_c values of the unimplanted TiN/Al and TiN/Ti/Al are 0.7 and 1.4 N, respectively, whereas that of the TiN/Ti/Ti-implanted Al sample is 4.1 N. It is evident that the critical load increases with the introduction of the interlayer and can be further improved by Ti ion implantation.

IV. FINITE ELEMENT MODELING

In our work, the ANSYS program is used to solve the highly nonlinear contact problem associated with elastic-plastic strain under the indenter. Different finite element models are used for our three samples: (a) TiN/Al, (b) TiN/Ti/Al, and (c) TiN/Ti/Ti-implanted Al. It is assumed that the film, interlayer, and substrate have permanent glues. The films and substrates are modeled as von Mises solids with discrete yielding followed by linear, isotropic work hardening. The properties of the materials are shown in Fig. 7, in which E is Young's modulus, Y is the yield strength, and E_r denotes the hardening modulus. Because of the nanoscale with undetermined mechanical properties, the interlayer and the modified layer are designated as elastic solids with the appropriate Young's moduli and Poisson's ratios. The indenter is a semicircle 2 μm in radius and with loads both in the x and y directions. Young's modulus of the indenter is set as 90 000, so that it is treated as a rigid body. The procedure is thus similar to a system scratched under a rigid particle. Each model comprises quadrilateral elements, and the element meshes near the contact zone and interlayer regions are refined to cope with the abrupt change in the modulus there. All the nodes along the substrate base are constrained from the motion in the y direction, and two sides

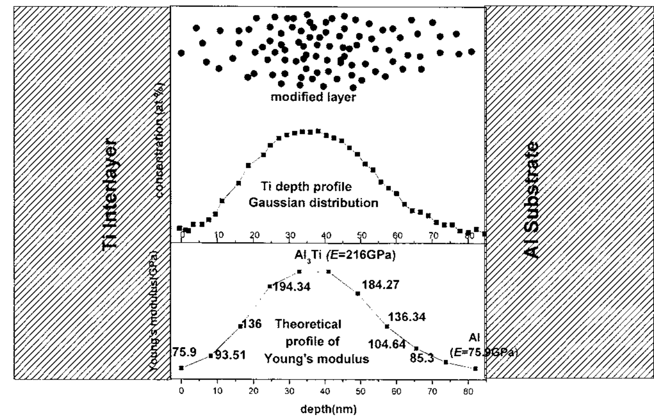

FIG. 8. Parameters of the modified layer in model (c).

are constrained from the motion in the x direction. The friction coefficient is set as 0.03 in all cases. The detailed sizes and material parameters of the models are listed in Table I. The data related to material properties are extracted from the literature.[18,19]

In the model of the third sample, TiN/Ti/Ti-implanted Al, a modified layer of 82 nm is added between the substrate and the interlayer according to experimental results. The modified layer is further divided into ten equal thin layers with detailed parameter setting, as illustrated in Fig. 8, which agrees with the Ti Gaussian distribution in the Al substrate as revealed by AES.

V. FEM RESULTS

It has been reported[20] that the base tensile stress is mainly responsible for the formation and extents of the longitudinal crack and that the film base shear stress can result in the film peeling off from the substrate.[20,21] Figure 9 compares the film base tensile stresses, shear stresses, and equivalent stresses of the three samples. The stress distributions of the different samples exhibit the main characteristic that the maximum values of stress are located below the rigid scratch. In other words, sharp changes and large stress exist in the interfacial region, in which minute cracks often nucleate from such stress discontinuity. Comparing the three samples, the stress distribution of the TiN/Ti/Ti-implanted

TABLE I. Material parameters of models.

	Materials	Thickness (μm)	Young's modulus (GPa)	Poisson's ratio	Yield stress (GPa)	Shear modulus (GPa)
Film	TiN	1.7	616	0.25	5	50
Substrate	Al	20	75.9	0.34	0.485	0.146
Interlayer	Ti	0.3	110	0.33	⋯	⋯
Modified layer[a]	Al ~Al_3Ti	0.082	75.9 ~ 216 ~ 75.9[a]	0.3	⋯	⋯

[a]The parameter setting is explained in Fig. 8.

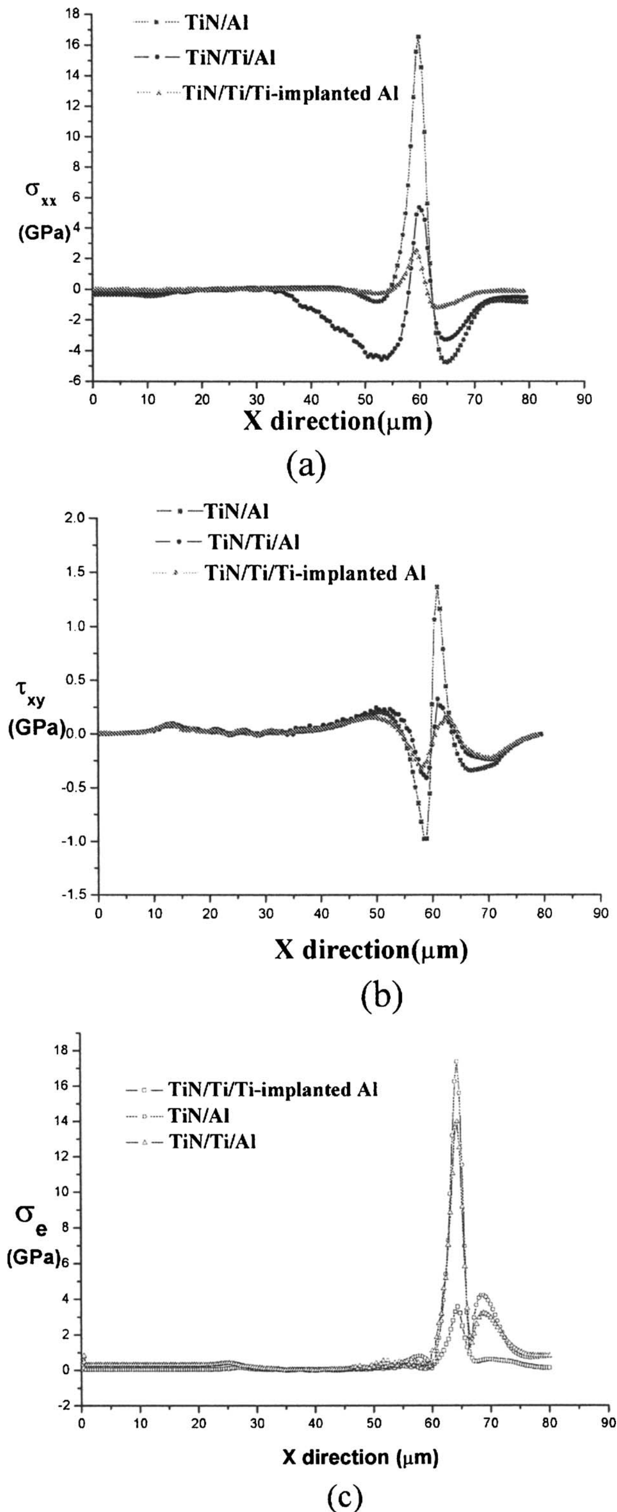

FIG. 9. (a) Film-base tensile stress σ_{xx}, (b) film base shear stress τ_{xy}, and (c) equivalent stress σ_e of the three samples.

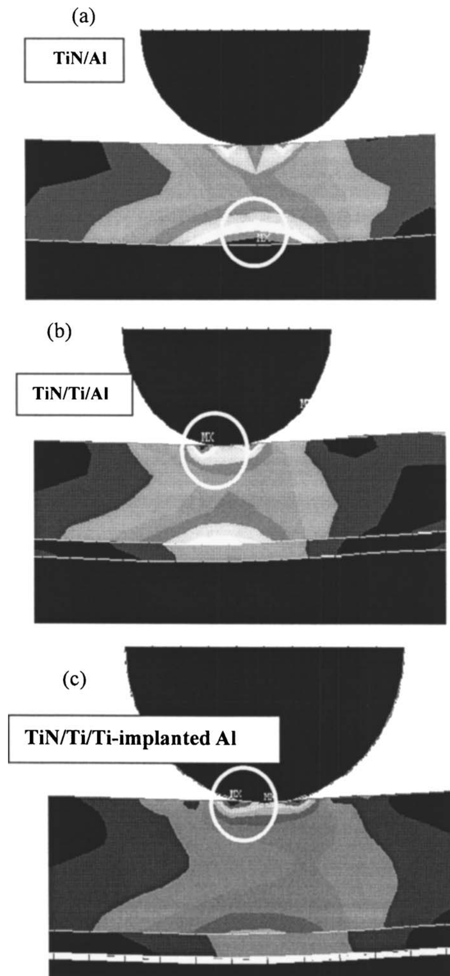

FIG. 10. Stress contours of (a) TiN/Al-, (b) TiN/Ti/Al-, and (c) TiN/Ti/Ti-implanted Al.

Al sample is smoother than that of the other two. That is, the cracks have relatively low probabilities to form at the interface.

Figure 10 shows parts of the stress contours of the three samples in the von Mises plots subjected to the same surface loading. As shown in Fig. 10(a), the maximum stress of the TiN/Al sample is at the interface between TiN and Al. Meanwhile, the stress contours are concentrated near the interfacial zone and are relatively sparse in the top region of the film surface. The results reveal that the interfacial region bears the main stress and the hard TiN film is not able to perform its function adequately to provide resistance to loadings. The common outcome is the formation of fractures near the interface due to the large stress. On the other hand, as illustrated in Figs. 10(b) and 10(c), the maximum stresses are located on the hard film surface just below the indenter when a Ti interlayer is introduced. The TiN films in these two samples thus play a bigger role in protecting the substrate. In addition, the stress contours of the TiN/Ti/Al sample are mostly concentrated near the top surface and then at the interface, but are sparse in the middle region of the film. Therefore, the TiN/Ti/Al sample still cannot effectively leverage the whole film to bear the loadings, but rather the stress disperses to the two sides of the film. The middle region of the film cannot provide good protection, thus leading to stress concentration at the interface. In contrast, the stress contours of the Ti-implanted sample, TiN/Ti/Ti-implanted Al, are sparser near the interface and have a relatively even distribution in the film region. This leads to a

gradual change in the stress near the interface. Hence, the sample is the best from the perspective of adhesion strength since it does not tend to form a fracture between the interface and the substrate. This outcome is corroborated by our experimental investigation.

VI. DISCUSSION

Both the FEM analysis and experiments demonstrate that the TiN/Ti/Ti-implanted Al sample shows the best mechanical characteristics. By means of Ti preimplantation, a modified layer with Al_3Ti is delineated without an obvious interface. Among the various types of aluminide in Al–Ti, Al_3Ti has the highest oxidation resistance,[22] resulting in the formation of an impervious layer of Al_2O_3 during the subsequent deposition of the Ti interlayer. It is beneficial to Ti diffusion from the Ti interlayer to the implanted layer and to the bonding between the two. Dyrda and Sayer[23] and Hu *et al.*[24] have suggested that the harder the substrate, the better is its adhesion to the substrate. The strengthened substrate thus provides the film with a relatively effective support to bear loadings and also contributes to the improved adhesion strength.

Scratching causes increased elastic and plastic deformation until failure occurs in the film. The common failure is delamination of the film at the interface because of the distinct differences in the mechanical properties between the film and the substrate. The modified layer with gradient properties can be a lattice-matched template and can provide the whole system with structural continuity. In addition, it also acts as a buffer layer to reduce the stress concentration near the interfacial zone. The propagation and development of cracks can be effectively inhibited to reduce failure. As shown in our study, during scratching, the modified layer helps to disperse the stress evenly to the whole film so that the hard TiN film can resist loadings more effectively.

VII. CONCLUSION

Compared to a Ti interlayer alone, preimplanting Ti ions into the aluminum substrate can further improve the adhesion strength of the deposited TiN film. The 82-nm-thick modified layer formed on the substrate provides better bonding with the Ti interlayer and improves the adhesion strength of the whole system. Combined with the Ti interlayer, it reduces the stress concentration around the interface. The scratch tests show that the L_c values of the TiN/Al-, TiN/Ti/Al-, and TiN/Ti/Ti-implanted Al samples are 0.7, 1.4, and 4.1 N, respectively. FEM simulations help to reveal the stress distributions near the interface, including film-base tensile stress σ_{xx}, shear stress τ_{xy}, and equivalent stress σ_e during the scratch. Both our numerical and experimental results confirm stress reduction, inhibition of crack formation, and propagation and consequently improves mechanical properties by using Ti preimplantation before the deposition of the Ti interlayer and the TiN layer.

ACKNOWLEDGMENTS

This work was jointly supported by the National Natural Science Foundation of China (No. 50271004), the City University of Hong Kong Direct Allocation (Grant No. 9360110), and the Scientific Effort of Shanghai Science and Technology Committee (0359nm005).

[1]R. Banerjee, R. Chandra, and P. Ayyub, Thin Solid Films **405**, 64 (2002).
[2]H. Holleck and V. Schier, Surf. Coat. Technol. **76/77**, 328 (1995).
[3]Y. Y. Guu and J. F. Lin, Surf. Coat. Technol. **85**, 146 (1996).
[4]E. A. Starke, Jr. and J. T. Staley, Prog. Aerosp. Sci. **32**, 131 (1996).
[5]L. M. Liu, S. Q. Wang, and H. Q. Ye, Acta Mater. **52**, 3681 (2004).
[6]R. Saha and W. D. Nix, Mater. Sci. Eng., A **319–321**, 898 (2001).
[7]G. S. Kim, S. Y. Lee, J. H. Hahn, B. Y. Lee, J. G. Han, J. H. Lee, and S. Y. Lee, Surf. Coat. Technol. **171**, 83 (2002).
[8]F. S. Shieu, L. H. Cheng, M. H. Shiao, and S. H. Lin, Thin Solid Films **311**, 138 (1997).
[9]I. A. Solodukhin, V. V. Khodasevich, V. V. Uglov, M. Brizuela, and J. I. Oñate, Surf. Coat. Technol. **142–144**, 1144 (2001).
[10]P. W. Shum, Z. F. Zhou, and K. Y. Li, Surf. Coat. Technol. **166**, 213 (2003).
[11]P. W. Shum, Z. F. Zhou, K. Y. Li, and C. Y. Chan, Thin Solid Films **458**, 203 (2004).
[12]H. H. Tong, O. R. Monterio, and I. G. Brown, Surf. Coat. Technol. **136**, 211 (2001).
[13]Z. M. Zeng, T. Zhang, X. B. Tian, B. Y. Tang, T. K. Kwok, and P. K. Chu, Surf. Coat. Technol. **128/129**, 236 (2000).
[14]P. K. Chu, S. Qin, C. Chan, N. W. Cheung, and L. A. Larson, Mat. Sci. Eng. Reports **17**, 207 (1996).
[15]P. K. Chu, B. Y. Tang, L. P. Wang, X. F. Wang, S. Y. Wang, and N. Huang, Rev. Sci. Instrum. **72**, 1660 (2001).
[16]S. T. Knight, P. J. Evans, and M. Samandi, Nucl. Instrum. Methods Phys. Res. B **119**, 501 (1996).
[17]D. Jawarani, J. P. Stark, H. Kawasaki, J. O. Olwolafe, C. C. Lee, J. Klein, and F. Pintchovski, J. Electrochem. Soc. **141**, 302 (1994).
[18]X. Cai and H. Bangert, Thin Solid Films **264**, 59 (1995).
[19]S. S. Nayak and B. S. Murty, Mater. Sci. Eng., A **367**, 218 (2004).
[20]I. A. Anderson and I. F. Collins, Wear **185**, 23 (1995).
[21]H. Djabella and R. D. Arnell, Thin Solid Films **235**, 156 (1993).
[22]M. Yamauchi, Y. Umakoshi, and T. Yamane, Philos. Mag. A **55**, 301 (1987).
[23]K. Dyrda and M. Sayer, Thin Solid Films **355/356**, 277 (1999).
[24]S. B. Hu, J. P. Tu, Z. Mei, Z. Z. Li, and X. B. Zhang, Surf. Coat. Technol. **141**, 174 (2001).